Charge Transfer between Water Molecules As the Possible Origin of the Observed Charging at the Surface of Pure Water

ARTICLE *in* JOURNAL OF PHYSICAL CHEMISTRY LETTERS · DECEMBER 2011

Impact Factor: 7.46 · DOI: 10.1021/jz2014852

6 AUTHORS, INCLUDING:

Robert Vácha
Masaryk University
47 PUBLICATIONS **1,950** CITATIONS
SEE PROFILE

Ondrej Marsalek
New York University
20 PUBLICATIONS **289** CITATIONS
SEE PROFILE

THE JOURNAL OF PHYSICAL CHEMISTRY Letters

Letter

pubs.acs.org/JPCL

Charge Transfer between Water Molecules As the Possible Origin of the Observed Charging at the Surface of Pure Water

Robert Vácha,[†] Ondrej Marsalek,[‡] Adam P. Willard,[§] Douwe Jan Bonthuis,[∥] Roland R. Netz,[⊥] and Pavel Jungwirth*,[‡]

[†]National Centre for Biomolecular Research, Faculty of Science and CEITEC - Central European Institute of Technology, Masaryk University Brno, Kamenice 5, 625 00 Brno-Bohunice, Czech Republic

[‡]Institute of Organic Chemistry and Biochemistry, Academy of Sciences of the Czech Republic and Center for Biomolecules and Complex Molecular Systems, Flemingovo nám. 2, 16610 Prague 6, Czech Republic

[§]Department of Chemistry and Biochemistry and Institute for Computational Engineering and Sciences, 1 University Station A5300, University of Texas at Austin, Austin, Texas 78712-1167, United States

[∥]Physik Department, Technische Universität München, 85748 Garching, Germany

[⊥]Fachbereich Physik, Freie Universität Berlin, Arnimalle 14, 14195 Berlin, Germany

ABSTRACT: Classical molecular dynamics simulations point to an anisotropy of water−water hydrogen bonding at the water surface. Approaching from the gas phase, a region of primarily dangling hydrogens is followed by dangling oxygens before the isotropic bulk region. Using ab initio calculations, we translate this hydrogen bonding anisotropy to charge transfer between water molecules, which we analyze with respect to both instantaneous and averaged positions of the water surface. Similarly to the oil/water interface, we show that there is a region of small net negative charge extending 0.2 to 0.6 nm from the Gibbs dividing surface in the aqueous phase. Using a simple continuum model, we translate this charge profile to a zeta potential, which acquires for realistic positions of the shear surface the same negative sign as that observed experimentally, albeit of a smaller absolute value.

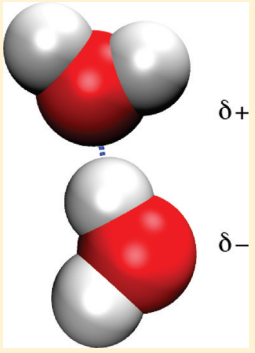

SECTION: Surfaces, Interfaces, Catalysis

The surface of water has distinctly different properties from the aqueous bulk, which can lead to an uneven distribution of the inherent water ions, hydronium and hydroxide, in the interfacial layer compared with the bulk.[1] It has been reported in several studies, that the surfaces of small water droplets as well as air bubbles and oil droplets in water carry a negative charge.[2−10] Although the molecular origin of this charge remains elusive (and may even differ from case to case), it has been repeatedly suggested that it is due to surface accumulation of OH^-.[5−10] However, the deduced surface charge density of −5 to −7 $\mu C/cm^2$ would represent a more than one million fold surface enhancement of hydroxide concentration in pure water.[9] This is in conflict with second harmonic generation (SHG),[11] photoelectron spectroscopy (PES),[12] and surface tension measurements[13] as well as with molecular simulations.[1,14,15] Moreover, it would be contradictory for any species to be strongly soluble (solubility of NaOH in water[16] is >1000 g/L) and extremely surface active at the same time.

In a recent paper, we suggested a different physical explanation for the origin of the negative charge at the water/oil interface.[17] Leaving aside the possibility that it could be due to accumulation of surface active impurities such as titratable fatty acids,[18] we focused on the potential effect of charge transfer between water molecules.[17,19,20] In the water dimer, the asymmetry of the hydrogen bond leads to a charge transfer of 0.002 to 0.02 e from the hydrogen accepting to the hydrogen donating water molecule,[21,22] as schematically depicted in Figure 1. In the isotropic environment of the aqueous bulk this effect cancels out on average, however, this is not necessarily true at the anisotropic interface.

We showed that at the oil/water interface there is indeed a nonzero charge profile due to the charge transfer between water molecules.[17] The interfacial water molecules have an increased number of unsaturated hydrogen bonds, the so-called dangling hydrogens and dangling oxygens,[23−27] which are not distributed isotropically. The top water layer has more dangling hydrogens leading to the positive charge due to the charge transfer. This is overcompensated by dangling oxygens in the layer below, so the cumulative charge changes sign about 3 Å below the Gibbs dividing surface (GDS) between water and oil and becomes negative up to ∼8 Å, after which it levels off to zero. As a result, in the aqueous region between 3 and 8 Å below the GDS, there is a region with a net negative charge, which could lead to

Received: November 10, 2011
Accepted: December 12, 2011

   dx.doi.org/10.1021/jz2014852 | J. Phys. Chem.Lett. 2012, 3, 107−111

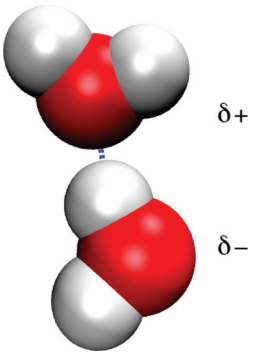

Figure 1. Schematic picture of the charge transfer from the hydrogen bond acceptor to the hydrogen bond donor in the water dimer. The charge transfer leaves the hydrogen bond acceptor molecule slightly positively charged ($\delta+$) and the hydrogen bond donor molecule slightly negatively charged ($\delta-$).

electrophoretic mobility of the oil particles toward the positive electrode.[17]

In the present study, we focus on charge transfer at the water/vapor interface. Using molecular dynamics (MD) simulations with empirical force fields we analyze the hydrogen bonding asymmetry at the surface of pure water employing both laboratory frame and intrinsic density profile analyses.[28,29] By means of ab initio MD simulations we demonstrate that instantaneous asymmetry in hydrogen bonding is indeed directly connected to charge transfer. Finally, using a simple continuum model of water surface we show that a region of negative charge in the interfacial layer of water, which is due to charge transfer between water molecules, gives rise to a small negative zeta potential for realistic positions of the effective shear surface.

Classical Molecular Dynamics. Classical MD simulation was performed using the GROMACS program package version 4.0.5.[30] The system was composed of 6000 water molecules placed in a prismatic cell of dimensions 4.0 × 4.0 × 30.0 nm yielding an infinite slab with thickness of ∼11 nm. After 10 ns of equilibration, a production run of 50 ns was carried out with a 2 fs time step. The canonical constant-volume (NVT) ensemble was employed keeping the system at ∼300 K using the V-rescaling thermostat with coupling constant of 1.0 ps.[31] The van der Waals and Coulomb interactions were cut off at 1.0 nm with the particle mesh Ewald (PME) method[32] applied to account for the long-range Coulomb interactions. The SPC/E water model[33] was employed with structure kept rigid using SETTLE algorithm.[34]

Ab Initio Molecular Dynamics. Ab initio molecular dynamics (AIMD) simulations based on density functional theory were performed using the CP2K simulation package.[35] We placed 216 water molecules in a 15 Å × 15 Å × 50 Å simulation cell. The size in the z direction together with a Poisson solver suitable for two periodic and one open dimension[36] allow simulation of a slab with two open surfaces. The Becke correlation functional was used together with the Lee−Yang−Parr exchange functional and the second generation of the Grimme dispersion correction (BLYP-D2).[37] Kohn−Sham orbitals were expanded in a triple-ζ Gaussian basis set with two additional polarization functions that was optimized for condensed molecular systems (molopt-TZV2P).[38] Electronic density was represented using plane waves with a cutoff of 280 Ry. Born−Oppenheimer dynamics was performed, and the self-consistent field cycle was converged to within 10^{-7} at each 0.5 fs MD step.

The initial condition was obtained from a classical MD simulation with the SPC/E force field. The system was simulated using AIMD for a total of 25 ps, and the first 2.5 ps of the ab initio trajectory were discarded as equilibration. The temperature of 300 K was imposed using a velocity rescaling thermostat, which generated the canonical ensemble with a time constant of 50 fs.[31] The charge density of the system was saved on the full resolution grid with dimensions 160 × 160 × 512 every 10 steps. This density was then decomposed into molecular charges using Bader population analysis as implemented by the Henkelman group.[39]

Continuum Hydrodynamic Model. Across the air−water interface, the viscosity drops from the water bulk value to the value in air, which is close to zero. To calculate the zeta potential, the viscosity profile across the interface is needed. The viscosity in the interfacial region is, in general, different from the bulk water viscosity. Approximating the viscosity profile by a step profile $\eta(z) = \eta_w(1 - \vartheta(z - z_0))$, which was found to be accurate for water at a hydrophobic surface,[40] the charges in the (effective) vapor phase cannot transfer any momentum to the air bubble. We take the coupling to the charges in the vapor phase into account by a surface friction coefficient, quantified by the slip length, b, equal to the viscosity divided by the friction coefficient. The Stokes equation reads

$$\nabla\eta(z)\nabla u_{||}(z) = - E_{||}\rho(z) \tag{1}$$

where $\eta(z)$ is the viscosity, $u_{||}(z)$ is the velocity parallel to the surface in response to an applied electric field $E_{||}$, and $\rho(z)$ is the charge density resulting from the charge transfer. Integrating once with respect to z and using the boundary condition that $\nabla u_{||}(z)$ and the integral over all charges vanish in the bulk fluid leads to

$$\eta(z)\nabla u_{||}(z) = - E_{||}F_{\perp}(z) \tag{2}$$

with $\nabla F_{\perp}(z) = \rho(z)$. Integrating eq 2 from a position z_w in the bulk water to z_0, where the viscosity vanishes, gives

$$u_{||}(z_0) - u_{||}(z_w) = \frac{E_{||}}{\eta_w}\int_{z_w}^{z_0} \rho(z)(z - z_0)\, dz \tag{3}$$

Now we apply the following boundary condition at $z = z_0$

$$u_{||}(z_0) = - b\nabla u_{||}(z)|_{z_0} \tag{4}$$

leading to

$$-u_{||}(z_w) = \frac{E_{||}}{\eta_w}\int_{z_w}^{z_0} \rho(z)(z - z_0 - b)\, dz \tag{5}$$

The zeta potential is defined as

$$\zeta = - \frac{\eta_w u_{||}(z_w)}{\varepsilon\varepsilon_0 E_{||}} \tag{6}$$

where ε_0 is the permittivity of vacuum and ε is the relative permittivity of water, for which we take $\varepsilon = 80$. Combining eqs 5 and 6 gives[41]

$$\zeta = \frac{1}{\varepsilon\varepsilon_0}\int_{z_w}^{z_0} \rho(z)(z - z_0 - b)\, dz \tag{7}$$

dx.doi.org/10.1021/jz2014852 | J. Phys. Chem.Lett. 2012, 3, 107−111

Equation 7 shows that the zeta potential essentially equals the first moment of the charge distribution. Note that we have formulated the theory in the moving frame of the bubble; that is, the velocity is zero in the vapor phase. In an experimental situation where the liquid is arrested, we therefore predict the vapor phase, that is, the bubble, to move.

Results and Discussion. We used the 50 ns classical MD simulation of the aqueous slab to analyze the balance between accepting and donating hydrogen bonds for water molecules at the water/vapor interface. A standard hydrogen bond definition, that is, O−O distance smaller than 0.35 nm and H−O−O angle smaller than 30°, was employed.[42] The system was cut in 0.05 nm thick layers parallel to interface, in which we assigned water molecules based on the instantaneous positions of their centers of mass. In the hydrogen bond counting performed over the whole trajectory, we added for each water molecule a value of +1 for each accepting hydrogen bond and a value of −1 for each donating hydrogen bond. The resulting value, that is, the excess of accepting over donating hydrogen bonds along the surface normal, is plotted in Figure 2. The

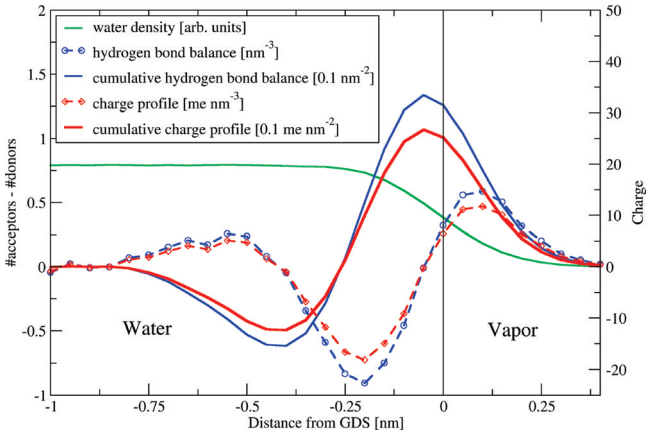

Figure 2. Hydrogen bond balance between accepted and donated hydrogen bonds at the water/vapor interface calculated in the 0.05 nm thick layers averaged over the whole production run and normalized per frame (blue). The cumulative profile shows the excess of hydrogen bonds present in water above (i.e., toward the vapor) the given point. The cumulative profiles are multiplied by a factor of 10 to fit in the same graph. Charge profile and its cumulative value (red) that originate from charge transfer is depicted with employed value of charge transfer 0.02 e per hydrogen bond. Note that there is a net negative surface charge of −1.3 me nm^{-2} at 0.4 nm below the GDS. For clarity, a water density profile in arbitrary units is also depicted.

corresponding cumulative sum is then the integral of this curve, that is, the total excess of accepting over donating hydrogen bonds in the system above a given depth. (By "above" we literarily mean "toward the vapor phase".)

Figure 2 shows that the hydrogen bond excess is positive above the GDS (being roughly at the position where the water density reaches half of its bulk value), but just below GDS (i.e., toward the water phase) it changes sign. The negative values peak at 0.2 nm below the GDS. The excess then becomes positive again at ∼0.4 nm, leveling off to zero (i.e., the value corresponding to the symmetric bulk) at <1 nm below the GDS. The cumulative values, that is, the integrals of the hydrogen bond excess from the vapor phase to a given depth in the interface, are first positive (around GDS) but become negative below the GDS with a peak of cumulative hydrogen bond excess of −0.06 nm^{-2} at 0.4 nm below the GDS.

Using the values of charge transfer per hydrogen bond of 0.002 to 0.04 e, estimated from ab initio calculations on small water clusters (dimer in particular),[21,22,43] we can aim at obtaining the corresponding charge profile and its cumulative sum (Figure 2). As in our previous study, we have employed here an intermediate value of charge transfer of 0.02 e per hydrogen bond.[17] The charge profile is then a "dressed" profile of the hydrogen bond excess, with the cumulative negative charge density peaking at a value of −0.0013 e nm^{-2} at 0.4 nm below the GDS. A similar, albeit somewhat smaller value was previously obtained also for the water/oil interface.[17] (Note that in ref 17 we plotted the *surface* charge density for 0.05 nm thick slices; therefore, a conversion factor of 1/0.05 should be applied to directly compare to the present data.)

The analysis in terms of density profiles of hydrogen bond excess or charge performs a lateral averaging that smears out local fluctuations due to surface roughness. The liquid−vapor phase boundary is made rough by thermal fluctuations that serve to smear out properties computed relative to the GDS. Furthermore, because the amplitude of interfacial fluctuations depends on the wave vector, the amount of smearing depends to some extent on system size. The instantaneous interface does not include contributions from fluctuations in interfacial position and is at each moment in contact with the vapor phase. Therefore, we have also constructed the hydrogen bond excess and charge profiles with respect to the instantaneous water surface using a recently designed procedure.[28] The results presented in Figure 3 show that the analysis with respect to the

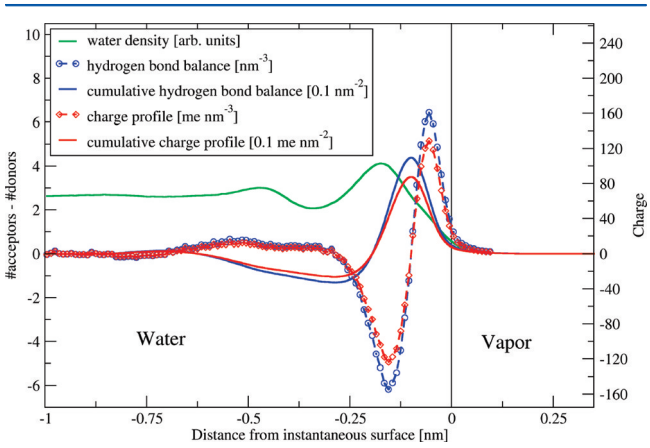

Figure 3. Instantaneous surface plot of excess and cumulative values of hydrogen bonds and the related charge profiles at the water/vapor interface. As in Figure 2, the cumulative profiles are multiplied by a factor of 10 to fit in the same graph, and a value of charge transfer 0.02 e per hydrogen bond was employed.

instantaneous surface enhances the hydrogen bond excess in the interfacial layer. Both the positive and negative peaks of the hydrogen bond excess increase several fold compared with the averaged values in Figure 2. Also, the cumulative excess becomes more pronounced, both on the positive side near the GDS and on the negative side between 0.2 and 0.6 nm below the GDS, with the negative region being now broader and about twice as deep. This effect directly translates to the charge profiles in which there is a rather broad region of negative cumulative charge density of more than 0.002 e nm^{-2} in absolute value at 0.2 to 0.4 nm below the GDS (Figure 3). This

dx.doi.org/10.1021/jz2014852 | J. Phys. Chem.Lett. 2012, 3, 107−111

charge thus has the same sign as that deduced from macroscopic measurements,[6,9] albeit its absolute value is smaller. Also, assuming a weak surface affinity of hydronium cations,[44] it is clear that this negative charge could be titrated out at acidic conditions, as observed in the experiment.[6,9]

The charge transfer effect at the water/vapor interface could, in principle, be directly obtained from AIMD simulations. However, classical MD simulations show that one needs nanosecond simulations of hundreds of water molecules to converge the hydrogen bond excess and, consequently, also the charge profiles. This is hardly feasible within AIMD; nevertheless, this method can be used to verify the above assumption concerning the relation between the hydrogen bond excess and charge transfer. To achieve this, it is sufficient to perform a much smaller and shorter simulation and extract charges on water molecules with different numbers of hydrogen bonds. Such a plot using the Bader charge analysis for water molecules with a balanced versus unbalanced number of donating and accepting hydrogen bonds is presented in Figure 4. As

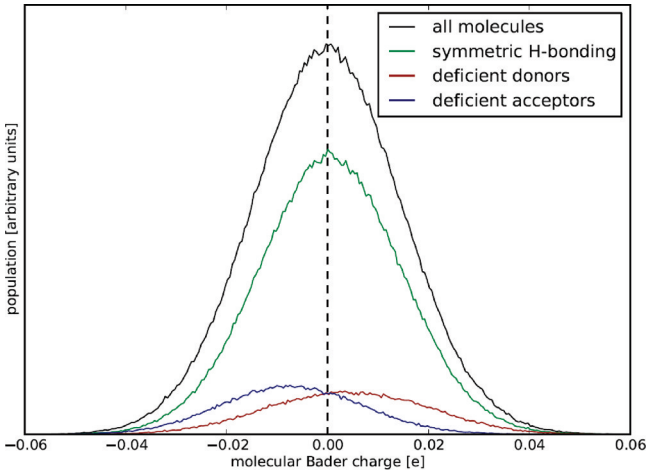

Figure 4. Correlation between H-bond asymmetry and charge on water molecules from AIMD.

expected, the total charge distribution as well as the charge distribution for water molecules with the same number of donating and accepting hydrogen bonds peak at zero, with distribution width of ∼0.02 e. More importantly, water molecules with (transient) hydrogen bond asymmetry also acquire an asymmetric charge distribution, as anticipated from the case of an isolated water dimer. This distribution, which is again rather broad, peaks at ±0.01 e for water molecules with an excess of donating or accepting hydrogen bonds. AIMD simulations thus confirm the relation between hydrogen bond asymmetry and charge transfer derived from the water dimer, agreeing also semiquantitatively on its absolute value.

In Figure 5a, we plot the zeta potential of an air bubble in water calculated from eq 7 using the instantaneous charge density profile (Figure 3). The position z_0 of the effective shear surface is varied between a position in vacuum, corresponding to an interfacial region with bulk viscosity, and a position up to several atomic layers inside the fluid, where all water properties are expected to reach bulk values.[23] Simultaneously varying the slip length b, we cover all different interfacial viscous properties that may be expected based on simulations of water at hydrophobic surfaces.[40] Clearly, the zeta potential depends strongly on the value of b. If the transfer charge density is

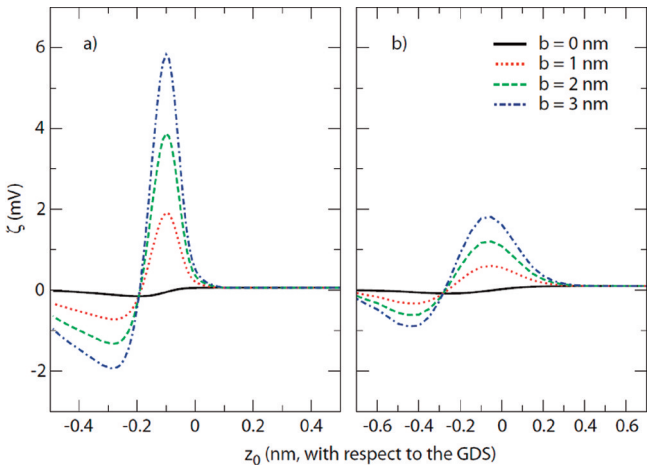

Figure 5. Zeta potential calculated from eq 7 as a function of the shear surface position z_0 using the charge density profile. The position z_0 is defined with respect to the Gibbs dividing surface GDS. Charge distribution from (a) instantaneous surface analysis (Figure 3) and (b) averaged surface analysis (Figure 2).

nonzero at the position of the effective shear surface z_0, then the bubble surface will not be stress-free because of the hydrogen bonds spanning across z_0. In addition, every air bubble has a nonzero slip length due to its curvature.[45] The effective slip length b is given as $1/b = 1/b_0 + 1/a$, where b_0 is the "intrinsic" slip length that is controlled by hydrogen bonds across the dividing surface as well as friction due to interacting water molecules and charges in the vapor and liquid phases, and a is the curvature of the bubble surface. Because of the large number of hydrogen bonds across the effective plane of shear, we expect b_0 to be small for $z_0 < 0.1$ nm. For $z_0 > 0.1$ nm, the water density is very small, and b_0 is expected to be large. For values of b of several nanometers, which we consider as an upper limit because this is the value for very hydrophobic surfaces, we find a zeta potential of several millivolts, that is, about an order of magnitude smaller than the zeta potential of about −35 mV measured for air bubbles in water.[6] Assuming that the transition from bulk-like to vapor-like hydrodynamic properties occurs effectively at one molecular layer beneath the surface, which is realistic in the view of the high self-diffusion constant of the top water layer found in MD simulations,[46,47] the zeta potential is negative. A negative peak is found at $z_0 = -0.28$ nm, that is, about one water layer below the surface, effectively leaving the air bubble with a net negative charge (compare the net charge at this depth in Figure 3). However, the zeta potential varies depending on the hydrodynamic properties of the interfacial region, and a positive peak is obtained at a very small value of $z_0 = -0.10$ nm. In addition, in Figure 5b, we show the zeta potential profiles with respect to the laterally averaged GDS (i.e., using charge profiles from Figure 2). Qualitatively, the graph shows the same features as Figure 5a, but the amplitude of the zeta potential is lower because of the smearing of the charge by lateral averaging. A calculation of the hydrodynamic flow that takes the laterally inhomogenous interfacial water structure into account is expected to produce results in between those presented in Figure 5a,b.

Conclusions. Classical MD simulations in conjunction with ab initio calculations point to a hitherto unappreciated charge transfer between water molecules at the surface of water, similarly to the situation at the oil/water interface discussed

dx.doi.org/10.1021/jz2014852 | J. Phys. Chem.Lett. 2012, 3, 107–111

recently.[17] Approaching from the gas phase, the charge transfer effect leads to a region of positive charge around the Gibbs dividing surface which, however, becomes overcompensated 0.2 to 0.6 nm below the GDS, leading to a net negative charge in this region. Deeper into the solution the net charge quickly approaches the bulk value of zero. A simple continuum model shows that this charge transfer leads to a nonzero zeta potential, which is negative amounting to about −2 mV for realistic positions of the effective shear surface about one water layer below the GDS. This is the same sign of zeta potential as that observed in the experiment,[6] however, the absolute value is significantly smaller. To improve the current model, the viscosity profile across the air−water interface would have to be explicitly calculated.

■ ACKNOWLEDGMENTS

We thank Branka Ladanyi, Janamejaya Chowdhary, and Dor Ben-Amotz for valuable discussions. P.J. acknowledges support from the Academy of Sciences (Praemium Academie) and the Czech Ministry of Education (grant LC512). Part of the research in Prague was supported via Project Z40550506. R.V. acknowledges financial support from the University of Cambridge and Churchill College, Cambridge and from European Regional Development Fund (CZ.1.05/1.1.00/02.0068 - project CEITEC). R.R.N. and D.J.B. acknowledge funding from the German Israeli Foundation for Scientific Research and Development (G.I.F.). A.P.W. acknowledges support from the U.S. Department of Energy (contract no. DE-AC02-05CH11231). O.M. acknowledges support from the IMPRS Dresden.

■ REFERENCES

(1) Buch, V.; Milet, A.; Vacha, R.; Jungwirth, P.; Devlin, J. P. *Proc. Natl. Acad. Sci. U.S.A.* **2007**, *104*, 7342−7347.
(2) Quincke, G. *Ann. Phys. Chem.* **1861**, *113*, 513.
(3) McTaggart, H. A. *Philos. Mag.* **1914**, *27*, 297.
(4) Graciaa, A.; Morel, G.; Saulner, P.; Lachaise, J.; Schechter, R. S. *J. Colloid Interface Sci.* **1995**, *172*, 131−136.
(5) Marinova, K. G.; Alargova, R. G.; Denkov, N. D.; Velev, O. D.; Petsev, D. N.; Ivanov, I. B.; Borwankar, R. P. *Langmuir* **1996**, *12*, 2045−2051.
(6) Takahashi, M. *J. Phys. Chem. B* **2005**, *109*, 21858−21864.
(7) Beattie, J. K.; Djerdjev, A. M. *Angew. Chem., Int. Ed.* **2004**, *43*, 3568−3571.
(8) Beattie, J. K. *Lab Chip* **2006**, *6*, 1409−1411.
(9) Beattie, J. K.; Djerdjev, A. M.; Warr, G. G. *Faraday Discuss.* **2009**, *141*, 31−39.
(10) Zilch, L. W.; Maze, J. T.; Smith, J. W.; Ewing, G. E.; Jarrold, M. F. *J. Phys. Chem. A* **2008**, *112*, 13352−13363.
(11) Petersen, P. B.; Saykally, R. J. *Chem. Phys. Lett.* **2008**, *458*, 255−261.
(12) Winter, B.; Faubel, M.; Vacha, R.; Jungwirth, P. *Chem. Phys. Lett.* **2009**, *474*, 241−247.
(13) Weissenborn, P. K.; Pugh, R. J. *J. Colloid Interface Sci.* **1996**, *184*, 550−563.
(14) Vacha, R.; Buch, V.; Milet, A.; Devlin, P.; Jungwirth, P. *Phys. Chem. Chem. Phys.* **2007**, *9*, 4736−4747.
(15) Mundy, C. J.; Kuo, I. F. W.; Tuckerman, M. E.; Lee, H. S.; Tobias, D. J. *Chem. Phys. Lett.* **2009**, *481*, 2−8.
(16) *CRC Handbook of Chemistry and Physics*; Lide, D. R., Ed.; Taylor & Francis: New York, 2005.
(17) Vacha, R.; Rick, S. W.; Jungwirth, P.; de Beer, A. G. F.; de Aguiar, H. B.; Samson, J. S.; Roke, S. *J. Am. Chem. Soc.* **2011**, *133*, 10204−10210.
(18) Vacha, R.; Buch, V.; Milet, A.; Devlin, J. P.; Jungwirth, P. *Phys. Chem. Chem. Phys.* **2008**, *10*, 332−333.
(19) Lee, A. J.; Rick, S. W. *J. Chem. Phys.* **2011**, *134*, 184507.
(20) Ben-Amotz, D. *J. Phys. Chem. Lett.* **2011**, *2*, 1216−1222.
(21) Glendening, E. D. *J. Phys. Chem. A* **2005**, *109*, 11936−11940.
(22) Khaliullin, R. Z.; Bell, A. T.; Head-Gordon, M. *Chemistry—Eur. J.* **2009**, *15*, 851−855.
(23) Stiopkin, I. V.; Weeraman, C.; Pieniazek, P. A.; Shalhout, F. Y.; Skinner, J. L.; Benderskii, A. V. *Nature* **2011**, *474*, 192−195.
(24) Buch, V. *J. Phys. Chem. B* **2005**, *109*, 17771−17774.
(25) Morita, A.; Hynes, J. T. *Chem. Phys.* **2000**, *258*, 371−390.
(26) Gragson, D. E.; Richmond, G. L. *J. Phys. Chem. B* **1998**, *102*, 3847−3861.
(27) Du, Q.; Superfine, R.; Freysz, E.; Shen, Y. R. *Phys. Rev. Lett.* **1993**, *70*, 2313−2316.
(28) Willard, A. P.; Chandler, D. *J. Phys. Chem. B* **2010**, *114*, 1954−1958.
(29) Chowdhary, J.; Ladanyi, B. M. *J. Phys. Chem. B* **2006**, *110*, 15442−15453.
(30) Hess, B.; Kutzner, C.; van der Spoel, D.; Lindahl, E. *J. Chem. Theory Comput.* **2008**, *4*, 435−447.
(31) Bussi, G.; Donadio, D.; Parrinello, M. *J. Chem. Phys.* **2007**, *126*, 014101.
(32) Darden, T.; York, D.; Pedersen, L. *J. Chem. Phys.* **1993**, *98*, 10089−10092.
(33) Berendsen, H. J. C.; Grigera, J. R.; Straatsma, T. P. *J. Phys. Chem.* **1987**, *91*, 6269−6271.
(34) Miyamoto, S.; Kollman, P. A. *J. Comput. Chem.* **1992**, *13*, 952−962.
(35) VandeVondele, J.; Krack, M.; Mohamed, F.; Parrinello, M.; Chassaing, T.; Hutter, J. *Comput. Phys. Commun.* **2005**, *167*, 103−128.
(36) Genovese, L.; Deutsch, T.; Goedecker, S. *J. Chem. Phys.* **2007**, *127*, 054704.
(37) Grimme, S.; Antony, J.; Ehrlich, S.; Krieg, H. *J. Chem. Phys.* **2010**, *132*, 154104.
(38) VandeVondele, J.; Hutter, J. *J. Chem. Phys.* **2007**, *127*, 114105.
(39) Tang, W.; Sanville, E.; Henkelman, G. *Journal of Physics-Condensed Matter* **2009**, *21*, 084204.
(40) Sendner, C.; Horinek, D.; Bocquet, L.; Netz, R. R. *Langmuir* **2009**, *25*, 10768−10781.
(41) Huang, D. M.; Cottin-Bizonne, C.; Ybert, C.; Bocquet, L. *Langmuir* **2008**, *24*, 1442−1450.
(42) Luzar, A.; Chandler, D. *Nature* **1996**, *379*, 55−57.
(43) Galvez, O.; Gomez, P. C.; Pacios, L. F. *J. Chem. Phys.* **2001**, *115*, 11166−11184.
(44) Jagoda-Cwiklik, B.; Cwiklik, L.; Jungwirth, P. *J. Phys. Chem. A* **2011**, *115*, 5881−5886.
(45) Joly, L.; Ybert, C.; Trizac, E.; Bocquet, L. *J. Chem. Phys.* **2006**, *125*, 204716.
(46) Taylor, R. S.; Dang, L. X.; Garrett, B. C. *J. Phys. Chem.* **1996**, *100*, 11720−11725.
(47) Townsend, R. M.; Rice, S. A. *J. Chem. Phys.* **1991**, *94*, 2207−2218.